IIETA International Information and Engineering Technology Association
Advancing the World of Information and Engineering

Journal Européen des Systèmes Automatisés
Vol. 59, No. 2, February, 2026, pp. 551-558
Journal homepage: http://iieta.org/journals/jesa

A Sensorless Speed Control Scheme for a Two-Wheel Electric Vehicle Driven by an Induction Motor Using Model Reference Adaptive System (MRAS) Based on Active Power

Fayssal E. Benmohamed[1*], Abdelmounaim Marouf[1], Ismail K. Bousserhane[2], Abdelfatah Nasri[2]

[1] Department of Electrical Engineering, Faculty of Technology, Salhi Ahmed University of Naama, Naama 45000, Algeria
[2] Smart Grids and Renewable Energies Laboratory, University Tahri Mohamed of Bachar, Bechar 08000, Algeria

Corresponding Author Email: benmohamed@cuniv-naama.dz

https://doi.org/10.18280/jesa.590224

Received: 21 November 2025
Revised: 4 February 2026
Accepted: 11 February 2026
Available online: 28 February 2026

Keywords:
electric vehicle, induction motor, Model Reference Adaptive System, implemented Field Oriented Control

ABSTRACT

In this research, we unveil a novel speed estimation schema for a two-wheel drive propulsion system. This paper presents a study on the Model Reference Adaptive System (MRAS) as applied to electric vehicles (EVs) with two independent wheels. Our proposed propulsion system is powered by two induction motor (IM) that drive both the front. We incorporate an electronic differential to calculate speed references for both wheels, which ensures robust control of the vehicle's behavior on the road. We implemented Field Oriented Control (FOC) to achieve excellent dynamic response along with precise and reliable control of both speed and torque. We simulated the MRAS estimator of our electric vehicle using the MATLAB Simulink environment, and the results were encouraging, demonstrating the effectiveness of our proposed control strategy.

1. INTRODUCTION

Modern control systems for electric motors play a crucial role in advancing industrial and transportation applications, especially as we move towards fully electrified propulsion systems. With the increasing demand for technologies that are high-performing, energy-efficient, and dependable, it's essential to create innovative solutions that blend energy efficiency, dynamic performance, and operational strength [1].

In the electric vehicle world, these innovations have led to better energy efficiency and a longer driving range, all while maintaining reliable performance in different conditions [2]. They've also shown to be quite effective in tackling the precision loss or instability problems that traditional methods often face at lower speeds [3].

The world of electric vehicles (EVs) has seen remarkable changes over the last few decades. We've moved from basic prototypes to highly advanced propulsion systems that feature cutting-edge digital controls and top-notch power electronics. The arrival of robust control strategies, like Field Oriented Control (FOC), has been a game-changer, allowing for impressive dynamic performance and precise management of speed and torque [3, 4]. FOC is well-known for its significant impact on high-performance induction motor (IM) drives. It allows for precise control of torque and flux, delivering dynamic performance that rivals that of separately excited DC motors [5].

Historically, early control methods leaned on simplified models and traditional techniques, but they ran into some challenges, especially when it came to low-speed or regenerative operations [3]. These challenges have sparked a lot of research into sensorless estimation, which helps cut costs and boost system reliability in tough industrial settings [4, 6].

This research primarily aims to accurately estimate state variables like speed and magnetic flux, all without relying on mechanical sensors [6]. This move towards “sensorless” systems is all about reducing possible failure points and enhancing the overall durability of drives [4]. In this context, Adaptive Observers and Model Reference Adaptive Systems (MRAS) have been shown to be quite effective at providing reliable estimations, even when faced with complex operating conditions [3]. Recent contributions have shown that MRAS schemes, especially those tailored for estimating rotor speed, can really enhance stability at low speeds and during regenerative operation [7].

In a broader sense, incorporating these estimation and adaptation algorithms into the electromechanical control environment has also had a positive impact on various other fields, including railway systems, wind turbines, and Ev’s. In these areas, achieving optimal energy conversion and management is crucial for enhancing overall system performance [1].

Various techniques are available for the estimation of Ev’s speed [5], rotor flux-based [8], MRAS based on reactive power, extended MRAS [4, 6, 9, 10], observer-based [11], rotor slot harmonics-based [12], and methods. Out of these. MRAS is popular due to its simplicity, requirement of less computation time, and good stability.

In this piece, we’re looking at the cutting-edge approaches to designing an estimation system for electric propulsion applications, with a special emphasis on sensorless speed control of an electric vehicle based on an IM using MRAS.

active power has been proposed as a reference model; the rotor speed will be estimated from an adaptive model.

2. DRIVE PROPULSION SYSTEM MODELING

The precise illustrates the electrical propulsion system of a two-wheel electric vehicle (EV) is shown in Figure 1. The system is powered by a battery that supplies energy to a central control system. This control unit generates control signals for two independent voltage-source inverters, each driving a three-phase electric motor connected to a wheel (left wheel and right wheel). The independent control of each wheel enables differential torque distribution, improving vehicle maneuverability and stability. The dashed lines and angle α represent the steering or wheel orientation with respect to the vehicle frame [4, 5, 10, 13, 14].

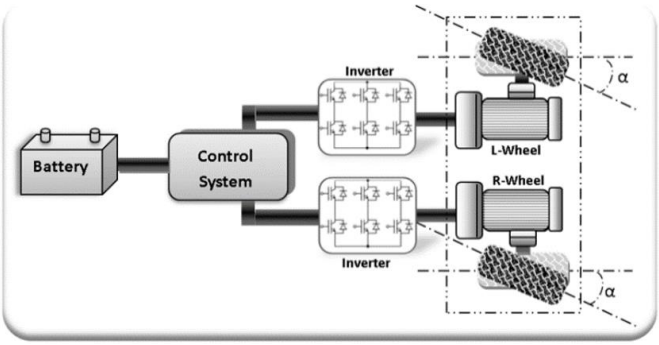

Figure 1. Electrical propulsion system of two wheels electric vehicle (EV) chain

2.1 Induction motor model

In the dq-reference frame that rotates synchronously with the rotor flux, the dynamic voltage equations for the three-phase squirrel-cage IM are represented as follows [1, 11].

$$\frac{d}{dt}\begin{bmatrix} i_{ds} \\ i_{qs} \\ \emptyset_{dr} \\ \emptyset_{qr} \end{bmatrix} = \begin{bmatrix} -A_1 & \omega_e & A_2 & A_3\omega_r \\ \omega_e & -A_1 & -A_3\omega_r & A_2 \\ A_4 & 0 & -A_5 & -\omega_{sl} \\ 0 & A_4 & \omega_{sl} & -A_5 \end{bmatrix} \begin{bmatrix} i_{ds} \\ i_{qs} \\ \emptyset_{dr} \\ \emptyset_{qr} \end{bmatrix} + \frac{1}{\sigma L_s}\begin{bmatrix} 1 & 0 \\ 0 & 1 \\ 0 & 0 \\ 0 & 0 \end{bmatrix}\begin{bmatrix} v_{ds} \\ v_{qs} \end{bmatrix} \quad (1)$$

and

$$\begin{bmatrix} i_{ds} \\ i_{qs} \end{bmatrix} = \begin{bmatrix} 1 & 0 & 0 & 0 \\ 0 & 1 & 0 & 0 \end{bmatrix} \begin{bmatrix} i_{ds} \\ i_{qs} \\ \emptyset_{dr} \\ \emptyset_{qr} \end{bmatrix} \quad (2)$$

where,

$$A_1 = \frac{1}{\sigma L_s}\left(R_s + \frac{L_m^2}{L_r\tau_r}\right), A_2 = \frac{1}{\sigma L_s}\left(\frac{L_m}{L_r\tau_r}\right), A_3 = \frac{1}{\sigma L_s}\left(\frac{L_m}{L_r}\right), A_4 = \frac{L_m}{\tau_r}, A_5 = \frac{1}{\tau_r}$$

The parameters of the induction motor are provided in Appendix.

2.2 Mechanical loads of the studied two wheels electric vehicle

The vehicle's mechanical load is made up of three resistive torques, which consist of:

1. Aerodynamic Torque T_{aero}

$$T_{aero} = \frac{1}{2}\rho S C_x R_r^2 . \omega_r^2 \quad (3)$$

2. Slope-related Torque T_{slope}

$$T_{slope} = Mg . \sin\alpha \, R_r \quad (4)$$

3. The maximal torque of the tire, which can oppose the motion, has the following expression

$$T_{max} = Mgf_r R_r \quad (5)$$

We obtain the total resistive torque:

$$T_{ev} = T_{slope} + T_{tyre} + T_{aero} \quad (6)$$

The way the traction system is modeled allows for the use of controls like vector control and speed control, which are essential for keeping the system stable overall [13, 14]. The EV parameters are included in the Appendix

3. INDIRECT FIELD ORIENTED CONTROL

The diagram in Figure 2 displays vector Control, which is often referred to as FOC, is crucial for maximizing the performance of drives. Its ease of use and swift dynamic response really set it apart [1]. This approach allows for decoupled control of torque and flux, similar to a DC machine, which is why it's been widely adopted in high-performance drives. The beauty of vector control lies in its excellent dynamic performance and its capability to independently control torque and flux through the d-axis (for flux) and q-axis (for torque) currents when things are steady [1].

To effectively implement IFOC, we start by transforming the three-phase stator quantities (abc) into a synchronous reference frame (dq) that is aligned with the rotor flux [4]. This method provides independent control over the flux using the direct axis current (ids) and the torque through the quadrature axis current (iqs). The correct orientation of the reference frame requires the slip frequency, calculated as [5].

$$\omega_s = \omega_m + \frac{L_m}{T_r} . \frac{i_{qs}}{\emptyset_r} \quad (7)$$

4. MODEL REFERENCE ADAPTIVE SYSTEM BASED ON ACTIVE POWER

The MRAS has gained traction in IM drives for sensorless control applications, primarily because it can accurately estimate speed and flux without relying on additional mechanical sensors [4]. In the active power based MRAS approach, the reference model calculates active power using stator currents and voltages, while the adjustable model derives the same variable based on rotor speed. The

difference between these two models is processed by an adaptation mechanism [15], often a PI controller, which adjusts the estimated rotor speed until everything converges smoothly [5, 10, 16].

This method stands out for its robustness and ease of use, as it avoids relying on flux models that can be quite sensitive to changes in parameters [9]. Furthermore, active power MRAS has been successfully implemented in electric vehicle propulsion, where it enhances the effectiveness of field-oriented control schemes by providing dependable speed estimation across various operating conditions [5]. You can find the overall structure of MRAS illustrated in Figure 3.

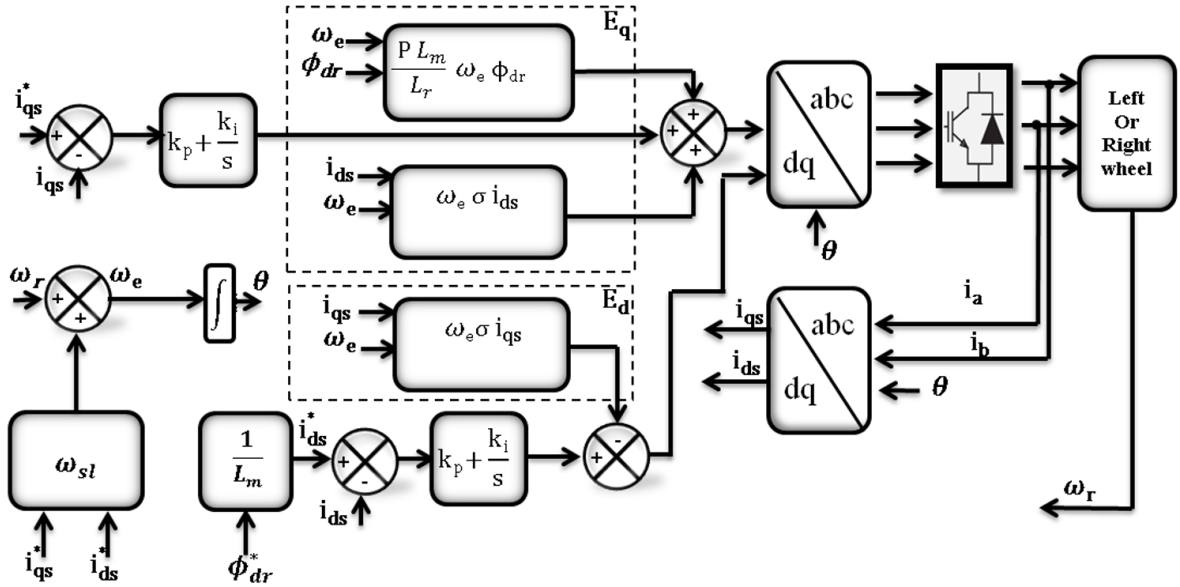

Figure 2. Schematic diagram of indirect flux vector control of induction motor (IM)

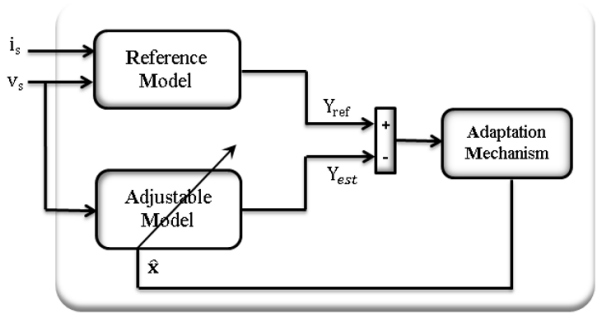

Figure 3. Basic configuration of Model Reference Adaptive System (MRAS)

The MRAS includes three essential blocks: the reference model, the adjustable model, and the adaptation mechanism as present in Figure 3 [15-18]. The reference model and adjustable model generate identical outputs, but they do it in distinct ways. To illustrate, the reference model follows a specific equation y_{ref}; whereas the adjustable model uses y_{est}. The error from the two models is directed to the adaptation mechanism, which produces the estimated quantity (x). To accurately estimate x from the MRAS, the reference model must be independent of x, while the adjustable model needs to be dependent on it [3, 17-20].

5. PROPOSED ESTIMATOR SYSTEM

Figure 4 shows the complete IM drive along with the proposed MRAS speed estimator. The speed estimation algorithm, which is outlined by a dotted line, consists of three primary blocks: the "Reference Model," the "Adjustable Model," and the "Adaptation Mechanism." We'll go into detail about the design of these blocks in the next subsections [3].

In the d-q synchronously rotating reference frame, the voltages equations of the IM can be articulated as [3]:

$$V_{qr} = R_s i_{qs} + \omega_e \sigma L_s i_{ds} + p\sigma L_s \dot{\imath_{qs}} + \frac{L_m}{L_r}(\omega_e \dot{\emptyset}_{dr} + p\emptyset_{qr}) \quad (8)$$

$$V_{ds} = R_s i_{ds} - \omega_e \sigma L_s i_{qs} + p\sigma L_s \dot{\imath_{ds}} - \frac{L_m}{L_r}(\omega_e \dot{\emptyset}_{qr} - p\emptyset_{dr}) \quad (9)$$

From a practical perspective, the instantaneous active power can provide really useful real-time data on the steady-state and dynamic behaviors of IM. This makes it a strong candidate for estimating IM parameters using a model reference adaptive control scheme. The active power for the IM can be calculated in a stationary reference frame using the following equation [5, 16]:

$$P_1 = (v_{ds} i_{ds} + v_{qs} i_{qs}) \quad (10)$$

Use of Eq. (10) also has the advantage of dispensing with the voltage sensors. Moreover, due to the filtering aspects, it is always easy to deal with the reference quantities.

Using Eqs. (8) and (9) in Eq. (10) and simplifying the instantaneous value of P:

$$P_2 = [R_s i_{qs} + \omega_e \sigma L_s i_{ds} + p\sigma L_s \dot{\imath_{qs}} + \frac{L_m}{L_r}(\omega_e \dot{\emptyset}_{dr} + p\emptyset_{qr}) i_{ds}] + [R_s i_{ds} - \omega_e \sigma L_s i_{qs} + p\sigma L_s \dot{\imath_{ds}} - \frac{L_m}{L_r}(\omega_e \dot{\emptyset}_{qr} - p\emptyset_{dr}) i_{qs}] \quad (11)$$

It's important to point out that the expressions for P mentioned above don't include stator resistance, which is a Substituting the condition $\emptyset_{dr} = L_m i_{ds}$ and $\emptyset_{qr} = 0$ for the (IFOC) IM drive, the more simplified expression P_3 to:

$$P_4 = \frac{L_m^{\,2}}{L_r}(\omega_{sl} + \widehat{\omega_r}) i_{ds} i_{qs} + R_s(i_{ds}^{\,2} + i_{qs}^{\,2}) \qquad (12)$$

Figure 4 shows proposed MRAS based on active power for speed estimation of IM, where a PI controller adjusts the estimated rotor speed to match the outputs of a reference model P_1 and an adjustable model P_4 using electrical active power error.

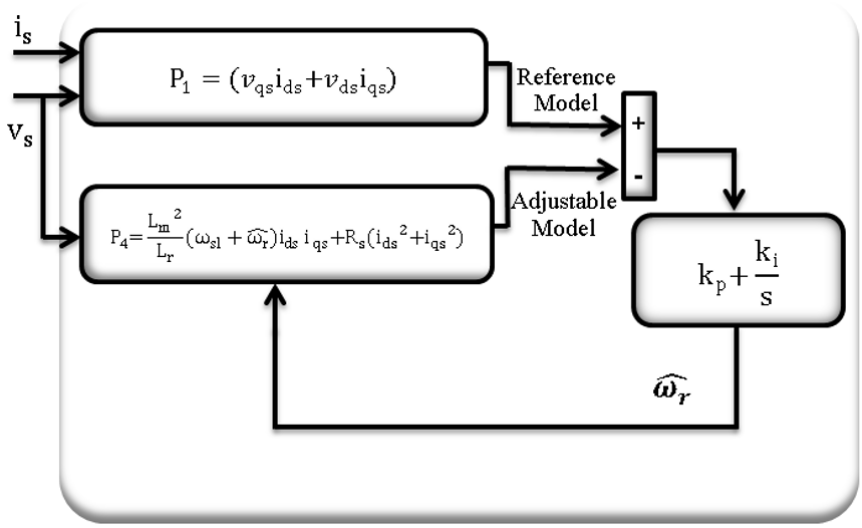

Figure 4. Proposed Model Reference Adaptive System (MRAS) based on active power for speed estimation

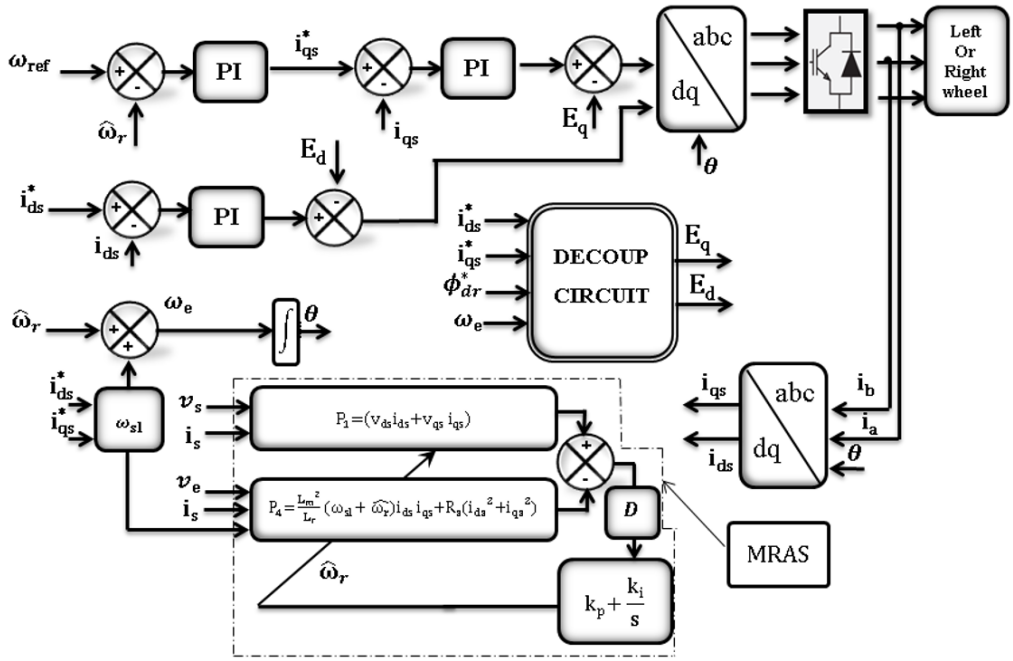

Figure 5. Vector controlled IM drive with Model Reference Adaptive System (MRAS) based speed estimator

The complete control system is presented in Figure 5, which combines a vector-controlled IM drive with a speed estimator based on the MRAS to provide accurate and dependable sensorless speed regulation.

6. SIMULATION RESULTS

In order to characterize the behavior of the drive wheel system, simulations were performed on MATLAB software and the following results were obtained.

6.1 Testing a 10% slop in movement on right-hand turns at a speed of 100 km/h

Figure 6 demonstrates the simulation results for a vehicle navigating a right-hand bend at a steady speed of 100 km/h. Between t = 2.5 s and t = 4.5 s, the vehicle climbs a 10% incline while maintaining the same speed. Thereafter, from t = 5 to 9 seconds, it continues moving through right-hand bends. We assume that both motors operate without any disturbances during these maneuvers. In these situations, the drive wheels take different paths, leading to varying

rotational speeds. Specifically, the right drive wheel turns more slowly than the left, as illustrated in subfigures:

a) Due to the applied motor torque, the right wheel speed increases quickly at first and closely tracks the reference speed. The speed stabilizes at about 100 km/h with minor fluctuations after one second. Due to load disturbances, there is a slight slowdown between 5 and 9 seconds, although tracking accuracy is still good. All things considered, the right wheel exhibits quick dynamic response and little sensitivity to changes in load.
b) Shows fine fluctuations around 100km/h. The estimated speed (red) and the reference speed (black) closely follow each other, with only a minimal tracking error. The speed control of the right wheel is accurate, maintaining steady tracking performance.
c) Similar profile as the right wheel; the left wheel estimated and reference speed rise rapidly to 100km/h. Both speed synchronize well, ensuring vehicle stability.
d) Small deviation between estimated and reference speed, similar to right wheel. Confirms proper tracking performance. MRAS estimator ensures steady regulation of wheel speed with minimal error.
e) The vehicle speed (linear combination of both wheel speeds) increases smoothly and reaches steady state after 2s. The maximum vehicle speed corresponds to the average of the two wheel speeds.
f) The resisting torque stays nearly constant, representing rolling resistance and aerodynamic drag. Drive torques must overcome this resistance to maintain motion.
g) After 1s, torque decreases as speed stabilizes. Between t = 4 s and t = 6 s, torque fluctuations are observed, possibly simulating disturbances or load changes associated with right-hand bend. High starting torque is required for acceleration; steady torque maintains speed; fluctuations reflect dynamic road/load conditions.
h) Direct flux quickly rises to 1 web and remains constant.

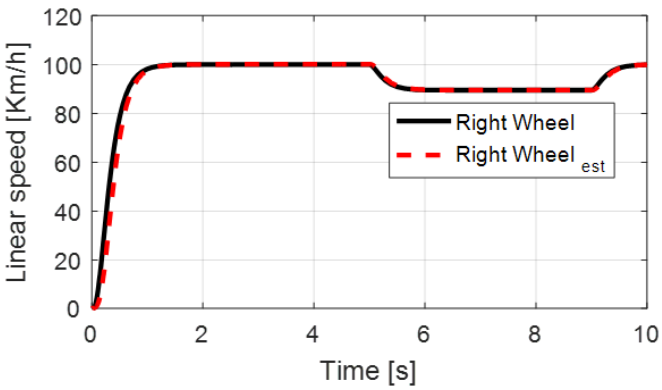

(a)-Linear speed of right wheel

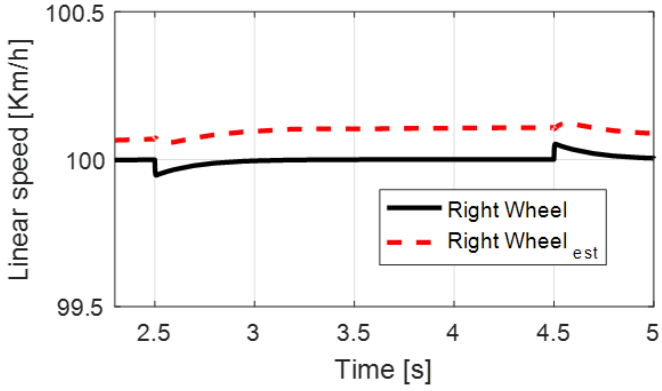

(b)-10 % slop at a steady speed of right wheel

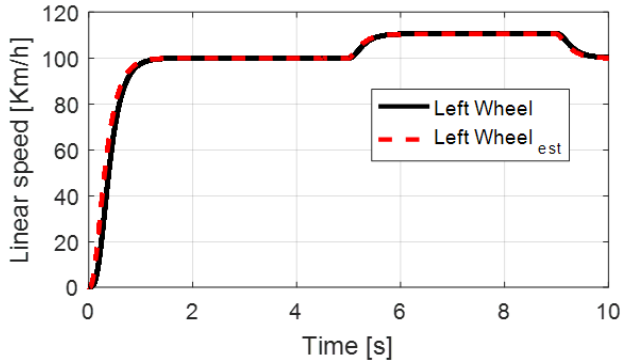

(c)-Linear speed of Left drive wheel

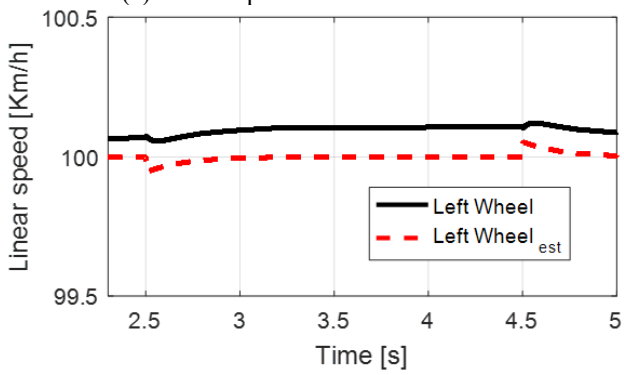

(d)-10 % slop at a steady speed of left wheel

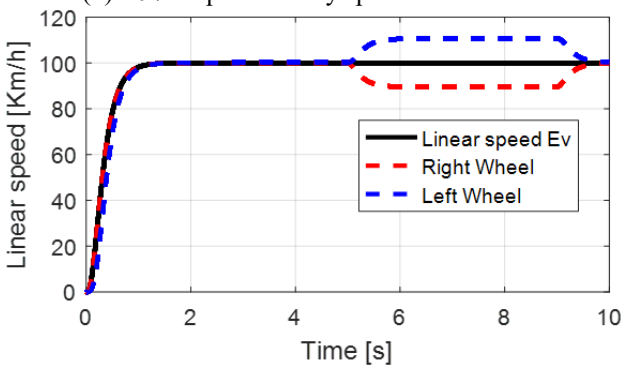

(e)-Linear speed of EV

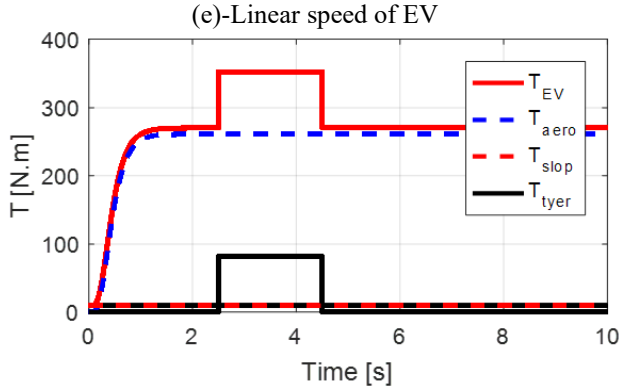

(f)-The torques of EV

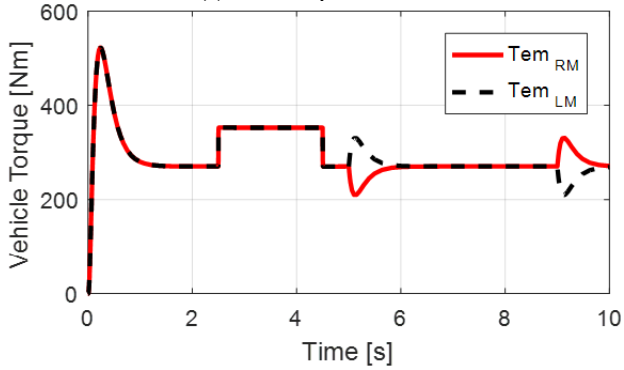

(g)-The torque of the right and left drive wheel

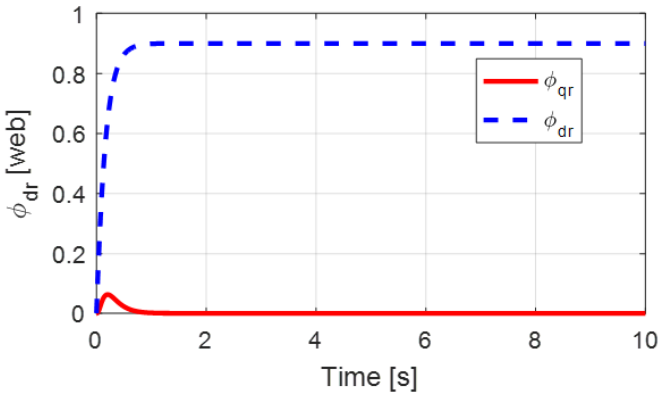

(h)-Quadrature and Direct flux

Figure 6. Simulation result for right hand-bands and 10 % slop at 100 km/h

6.2 Testing acceleration and deceleration with 10% slop

Figure 7 shows the speed profile displays repeated periods of acceleration, constant speed, and slowdown during the time span of 0 to 10 seconds. In the first second, the speed rises quickly from 0 km/h to roughly 40 km/h, after which it stays almost constant until about 2.5 s. It accelerates again to reach roughly 80 km/h by 3.5 s, followed by another steady-speed phase until about 4.5 s. After that, the speed rises to its maximum value of roughly 120 km/h at 5.5 s and stays virtually steady until 6.5 s. After a brief period of constant speed, there is a smooth deceleration phase during which the speed drops from 120 km/h to roughly 50 km/h between 6.5 and 8 seconds. Finally, the speed drops sharply from 50 km/h to 0 km/h between 9 s and 10 s, indicating a complete stop of the system and confirming controlled acceleration and deceleration behavior throughout the driving cycle.

a) depicts the linear speed of the right wheel as a function of time throughout sequential acceleration and deceleration phases with a 10% slop. Good estimation accuracy is indicated by the tight relationship between the estimated speed (red dashed line) and the actual measured speed (solid black line). The speed of the car rises gradually, peaks at about 120 km/h, and then gradually drops. Minor variations between the true and predicted speeds arise largely during rapid transitions, which is expected due to system dynamics and estimation delays.

b) This zoomed-in plot focuses on a brief time interval around the maximum speed. It draws attention to the tiny discrepancy between the estimated and observed speeds. The anticipated speed is slightly greater than the real speed, but the error remains quite minor (within a few tenths of km/h). This demonstrates that even in steady-state high-speed situations, the estimating method is still dependable.

c) The various torque components operating on the vehicle are depicted in this diagram. The electric vehicle torque T_{EV} (red line) increases during acceleration phases to counteract resistive torques. The aerodynamic torque T_{aero} (blue dashed line) increases with speed, becoming dominating at high velocities. The torque of the slope T_{slop} (black line) appears briefly, indicating a change in road incline. The torque of the tires T_{tyer} (red dashed line) is still rather tiny. Overall, the acceleration, cruising, and deceleration behavior seen in the speed graphs may be explained by the balance between these torques.

d) The direct flux $\emptyset_{dr}$ progression is seen in this graphic. And quadrature flux $\emptyset_{qr}$. The direct flux rapidly increases and stabilizes around its maximum value, showing a fast system reaction. On the other hand, the quadrature flux stays near zero. This implies that the system is stable and effectively controlled during the drive cycle.

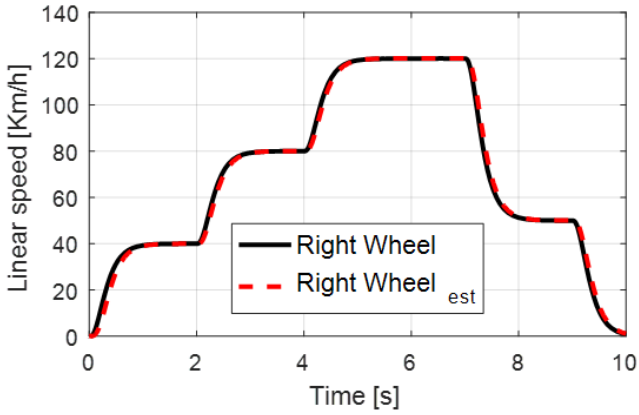

(a)- Linear speed of the right wheel

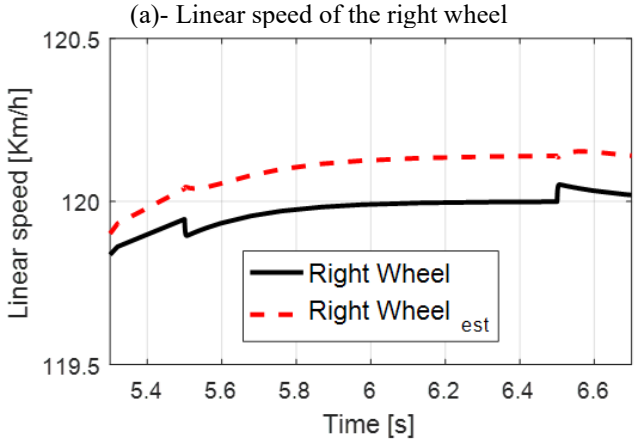

(b)- Zoomed view of linear speed (estimation accuracy)

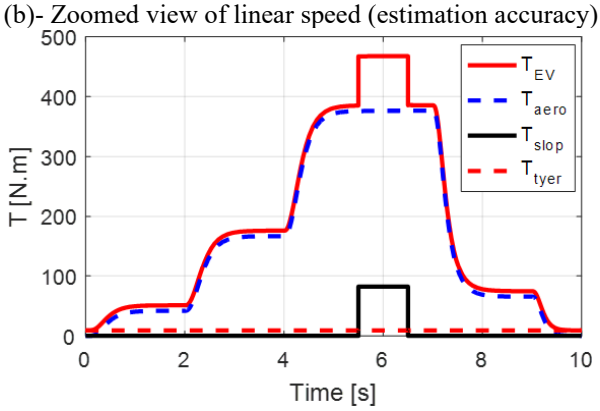

(c)- Torque components over time

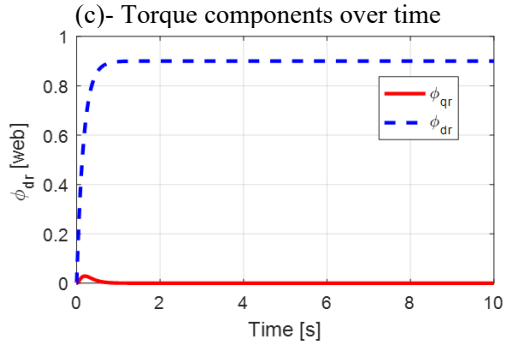

(d)- Driver and ground flux

Figure 7. Testing acceleration and deceleration with 10% slop

Global Interpretation

- The vehicle accelerates rapidly and reaches its target speed in 2 s.
- Both drive wheels track their reference speeds very accurately, with negligible tracking error, and the estimated speeds closely follow the reference speeds.
- When a resisting torque is applied, the system shows good disturbance rejection: only small speed dips occur, and stability is preserved.
- The torque distribution is well balanced between the left and right wheels, ensuring no wheel slip.
- Overall, the active power MRAS-based estimator strategy demonstrates fast dynamic response, accurate speed estimation, and strong robustness against external disturbances.
- Results confirm accurate modeling, stable control, and efficient, reliable vehicle performance during acceleration and deceleration.

A simplified qualitative comparison of Model Reference Adaptive System (MRAS)-based control strategies is presented in the Appendix.

7. CONCLUSIONS

In this paper, the research highlights the potential for improving the stability of two-wheel vehicles by using two independent drive wheels for motion, all through a MRAS based on Active Power. The study examines a control method applied to an EV, utilizing MRAS estimator to ensure safe driving on slopes. The MATLAB simulation results demonstrate that this estimate structure enables a robust speed control loop, achieving excellent dynamic performance in electric vehicles. The proposed MRAS-based model ensures precise speed estimation and regulation of the drive wheels under both flat and curved road conditions. The estimated wheel speeds closely track the reference speeds, maintaining high accuracy. Furthermore, road inclinations do not adversely affect the stability of the drive motors, highlighting the reliability and robustness of the proposed estimator and control strategy.

REFERENCES

[1] Pal, A., Kumar, R., Das, S. (2016). Sensorless speed control of induction motor driven electric vehicle using model reference adaptive controller. Energy Procedia, 90: 540-551. https://doi.org/10.1016/j.egypro.2016.11.222

[2] Dehghan-Azad, E., Gadoue, S., Atkinson, D., Slater, H., Barrass, P., Blaabjerg, F. (2016). Sensorless control of IM for limp-home mode EV applications. IEEE Transactions on Power Electronics, 32(9): 7140-7150. https://doi.org/10.1109/TPEL.2016.2627685

[3] Maiti, S., Chakraborty, C., Sengupta, S. (2009). Simulation studies on model reference adaptive controller based speed estimation technique for the vector controlled permanent magnet synchronous motor drive. Simulation Modelling Practice and Theory, 17(4): 585-596. https://doi.org/10.1016/j.simpat.2008.08.017

[4] Mapelli, F.L., Tarsitano, D., Cheli, F. (2017). MRAS rotor resistance estimators for EV vector controlled induction motor traction drive: Analysis and experimental results. Electric Power Systems Research, 146: 298-307. https://doi.org/10.1016/j.epsr.2017.02.005

[5] Kojabadi, H.M. (2009). Active power and MRAS based rotor resistance identification of an IM drive. Simulation Modelling Practice and Theory, 17(2): 376-389. https://doi.org/10.1016/j.simpat.2008.09.014

[6] Korzonek, M., Tarchala, G., Orlowska-Kowalska, T. (2019). A review on MRAS-type speed estimators for reliable and efficient induction motor drives. ISA Transactions, 93: 1-13. https://doi.org/10.1016/j.isatra.2019.03.022

[7] Pattanayak, D.P. (2019). A study of Mras based speed estimation of sensorless induction motor using MATLAB and Simulink modelling. Journal of Urban and Environmental Engineering, 13(2): 246-256. https://doi.org/10.4090/juee.2019.v13n2.246256

[8] Hurst, K.D., Habetler, T.G., Griva, G., Profumo, F. (2002). Zero-speed tacholess IM torque control: Simply a matter of stator voltage integration. IEEE Transactions on Industry Applications, 34(4): 790-795. https://doi.org/10.1109/28.703975

[9] Chakraborty, C., Ta, M.C., Hori, T. (2003). Speed sensorless, efficiency optimized control of induction motor drives suitable for EV applications. IECON'03. 29th Annual Conference of the IEEE Industrial Electronics Society (IEEE Cat. No. 03CH37468), 1: 913-918. https://doi.org/10.1109/IECON.2003.1280105

[10] Maiti, S., Chakraborty, C. (2010). A new instantaneous reactive power based MRAS for sensorless induction motor drive. Simulation Modelling Practice and Theory, 18(9): 1314-1326. https://doi.org/10.1016/j.simpat.2010.05.005

[11] Abu-Rub, H., Guzinski, J., Krzeminski, Z., Toliyat, H.A. (2003). Speed observer system for advanced sensorless control of induction motor. IEEE Transactions on Energy Conversion, 18(2): 219-224. https://doi.org/10.1109/TEC.2003.811735

[12] Ferrah, A., Bradley, K.G., Asher, G.M. (1992). Sensorless speed detection of inverter fed induction motors using rotor slot harmonics and fast Fourier transform. In PESC'92 Record. 23rd Annual IEEE Power Electronics Specialists Conference, Toledo, Spain, pp. 279-286. https://doi.org/10.1109/PESC.1992.254661

[13] Nasri, A., Gasbaoui, B., Fayssal, B.M. (2016). Sliding mode control for four wheels electric vehicle drive. Procedia Technology, 22: 518-526. https://doi.org/10.1016/j.protcy.2016.01.111

[14] Nasri, A., Gasbaoui, B., Fayssal, B.M. (2016). Novel four wheel drive propulsion system control using backstepping strategy. Procedia Technology, 22: 509-517. https://doi.org/10.1016/j.protcy.2016.01.110

[15] Benmohamed, F.E., Bousserhane, I.K., Kechich, A., Bessaih, B., Boucheta, A. (2016). New MRAS secondary time constant tuning for vector control of linear induction motor considering the end-effects. COMPEL-The International Journal for Computation and Mathematics in Electrical and Electronic Engineering, 35(5): 1685-1723. https://doi.org/10.1108/COMPEL-07-2015-0263

[16] Maiti, S., Chakraborty, C., Sengupta, S. (2007). Adaptive estimation of speed and rotor time constant for the vector controlled induction motor drive using

reactive power. In IECON 2007-33rd Annual Conference of the IEEE Industrial Electronics Society, Taipei, Taiwan, pp. 286-291. https://doi.org/10.1109/IECON.2007.4460396

[17] Vas, P., Stronach, A.F., Neuroth, M. (1998). Application of conventional and AI-based techniques in sensorless high-performance torque-controlled induction motor drives. In IEE Colloquium on Vector Control Revisited, pp. 8-1. https://doi.org/10.1049/ic:19980063

[18] Behloul, R., Mazouz, L., Boudiaf, M., Benmohamed, F.E. (2024). Enhancing wind energy conversion system performance via sliding mode control and parameter estimation with PI-MRAS. Journal Européen des Systèmes Automatisés, 57(2): 477. https://doi.org/10.18280/jesa.570217

[19] Omari, A., Ismail Khalil, B., Hazzab, A., Bouchiba, B., Benmohamed, F.E. (2019). Real-time implementation of MRAS rotor time constant estimation for induction motor vector control based on a new adaptation signal. COMPEL-The International Journal for Computation and Mathematics in Electrical and Electronic Engineering, 38(1): 287-303. https://doi.org/10.1108/COMPEL-03-2018-0133

[20] Özdemir, S. (2020). A new stator voltage error-based MRAS model for field-oriented controlled induction motor speed estimation without using voltage transducers. Electrical Engineering, 102(4): 2465-2479. https://doi.org/10.1007/s00202-020-01043-1

NOMENCLATURE

EV	Electric vehicle
IM	Induction motor
MRAS	Model Reference Adaptive System
FOC	Field Oriented Control
IFOC	Indirect Field Oriented Control
a, b, c	Three-phase stator reference frame
d, q	Direct–Quadrature reference frame
v_{ds}, v_{qs}	Stator voltages in the d–q reference frame
i_{ds}, i_{qs}	Stator currents in the d–q reference frame
$\emptyset_{ds}, \emptyset_{qs}$	Stator flux components in the d–q reference frame
$\emptyset_r$	Rotor flux
R_s	Stator resistance
R_r	Rotor resistance
L_s	Stator inductance
L_r	Rotor inductance
L_m	Mutual inductance
ω_s	Synchronous angular speed
ω_r	Rotor angular speed
$\widehat{\omega_r}$	Estimated rotor angular speed
ω_{sl}	Slip angular speed
T_{EV}	Electric vehicle traction torque
T_{aero}	Aerodynamic torque
T_{slop}	Slope-related torque
T_{tyer}	Tire resisting torque
J	Equivalent moment of inertia
f	Viscous friction coefficient
α	Road slope angle
P	Instantaneous active power
PI	Proportional–Integral controller
K_p	Proportional gain
K_i	Integral gain
$\emptyset_d$	Direct-axis flux
$\emptyset_q$	Quadrature-axis flux
θ	Electrical angle
σ	Coefficient of dispersion
R_{roy}	Wheel radius
g	Gravitational acceleration
M	Vehicle mass
ρ	Air density
S	Vehicle frontal area
C_x	Aerodynamic drag coefficient

APPENDIX

σ is the coefficient of dispersion is given by [13] :

$$\sigma = 1 - \frac{L_m^2}{L_s L_r}$$

Table 1. Simplified qualitative comparison of Model Reference Adaptive System (MRAS)-based control strategies

Criterion	MRAS-Based Active Power	MRAS-Based Reactive Power	MRAS-Based Flux
Tracking performance	High	Medium–High	High
Overshoot / oscillations	Low	Low–Medium	Low
Steady-state error	Very low	Low	Low
Implementation complexity	Medium	Medium	High

Table 2. Parameters of induction motor (IM) [13]

Parameter	Value	Unit
R_r	0.003	Ω
R_s	0.0044	Ω
L_r	494.9e-6	H
L_s	496.1e-6	H
L_m	482e-6	H
f	50	Hz
P	2	-
J	1.1	Kg.m^2

Table 3. Parameters of EV [13]

Parameter	Value	Unit
R_{roy}	0.25 – 0.30	m
g	9.806	m/s²
f	0.015	N·m·s/rad
M	1000	Kg
ρ	1.225	kg/m³
S	0.5 – 0.7	m²
C_x	0.7 – 0.9	-
α	0 ‑ 10°	Rad